

---

# Physics-Informed Diffusion Models

---

**Jan-Hendrik Bastek**

Department of Mechanical  
and Process Engineering  
ETH Zurich  
jbastek@ethz.ch

**WaiChing Sun**

Department of Civil Engineering  
& Engineering Mechanics  
Columbia University  
wsun@columbia.edu

**Dennis M. Kochmann**

Department of Mechanical  
and Process Engineering  
ETH Zurich  
dmk@ethz.ch

## Abstract

Generative models such as denoising diffusion models are quickly advancing their ability to approximate highly complex data distributions. They are also increasingly leveraged in scientific machine learning, where samples from the implied data distribution are expected to adhere to specific governing equations. We present a framework to inform denoising diffusion models on underlying constraints on such generated samples during model training. Our approach improves the alignment of the generated samples with the imposed constraints and significantly outperforms existing methods without affecting inference speed. Additionally, our findings suggest that incorporating such constraints during training provides a natural regularization against overfitting. Our framework is easy to implement and versatile in its applicability for imposing equality and inequality constraints as well as auxiliary optimization objectives.

## 1 Introduction

Denoising diffusion models [1] are generative models that have gained popularity due to their success in learning intricate data distributions across various modalities, including images [2, 3, 4], videos [5, 6], graphs [7, 8], text [9, 10], and audio waveforms [11]. Originally popularized within the image generation community, their outstanding representation abilities are also increasingly leveraged in the context of *scientific machine learning*. Diffusion models have been used, among others, to upscale low-fidelity data to reduce computational costs [12], design new molecules [13] or materials [14, 15] with desired properties, or generate metamaterial unit cells tailored to a given stress-strain response in complex mechanical settings [16].

A common thread of all those applications is the explicit knowledge of the underlying governing equations, which the implied distribution must obey. Often, the training data does not stem from experimental observations but is rather generated by numerical simulations, which ensure that those equations are fulfilled. Nevertheless, diffusion models are traditionally trained on a purely *data-driven* objective [14, 17, 16, 18, 19, 20, 21], and hence do not strictly enforce the intrinsic constraints during model training. Consequently, samples generated from such models may be statistically aligned with the training data but may not meet the required precision in scientific applications, where adherence to the underlying physics is crucial for deployment [22].

More recently, efforts have been made to ensure that samples generated from the learned distribution conform to the known constraints, e.g., in the form of ordinary [23] or partial differential equations (PDEs) [12, 22], human motion imitation [24], or manufacturability of proposed designs [25]. This has been achieved primarily by considering some form of gradient-based optimization or projection methods during inference. We here propose a different approach and directly incorporate constraints within the training process. Instead of correcting predictions after sampling from the model, this allows us to directly embed constraints into the proven representation strength of diffusion models and to draw synergies between the domains of physics-informed neural networks [26] and generative modeling, which we hence term *physics-informed diffusion models* (PIDM).

**Contributions.** We make the following key contributions: **(i)** We present a novel, theoretically motivated approach that informs denoising diffusion models on PDE constraints of generated samples during model training, and we demonstrate via rigorous numerical experiments that our framework reduces the PDE residual by 1-2 orders of magnitude compared to state-of-the-art methods. **(ii)** Interestingly, the additional training objective does *not* necessarily compromise the data likelihood, instead, we present evidence that it acts as an effective regularization against overfitting. **(iii)** Our framework is simple to implement in existing diffusion model architectures and the increased computational cost during training is minimal. Inference is unaffected and previous “post-processing” methods can still be applied, if required. **(iv)** While we focus on PDEs as a sophisticated type of equality constraint, our framework is equally applicable to other equality and inequality constraints as well as auxiliary optimization objectives.

## 2 Background

### 2.1 Denoising diffusion models

Denoising diffusion models are one of the state-of-the-art generative models [2, 27, 28] that learn to gradually convert a sample of a simple prior, typically a unit Gaussian, to a sample from a generally unknown data distribution  $q(\mathbf{x})$ . The idea is to introduce a fixed *forward diffusion process* that incrementally adds Gaussian noise to a given data sample  $\mathbf{x}_0 \sim q(\mathbf{x})$ , following variance schedule  $\{\beta_t \in (0, 1)\}_{t=1}^T$  over  $T$  steps, defined as

$$q(\mathbf{x}_{1:T}|\mathbf{x}_0) = \prod_{t=1}^T q(\mathbf{x}_t|\mathbf{x}_{t-1}), \quad q(\mathbf{x}_t|\mathbf{x}_{t-1}) = \mathcal{N}(\mathbf{x}_t; \sqrt{1 - \beta_t}\mathbf{x}_{t-1}, \beta_t \mathbf{I}). \quad (1)$$

To generate new samples, we consider the *reverse process*,

$$q(\mathbf{x}_{0:T}) = p(\mathbf{x}_T) \prod_{t=1}^T q(\mathbf{x}_{t-1}|\mathbf{x}_t), \quad q(\mathbf{x}_{t-1}|\mathbf{x}_t) = \mathcal{N}(\mathbf{x}_{t-1}; \boldsymbol{\mu}(\mathbf{x}_t, t), \boldsymbol{\Sigma}(\mathbf{x}_t, t)), \quad (2)$$

in which we approximate the unknown true inverse conditional distribution  $q(\mathbf{x}_{t-1}|\mathbf{x}_t)$  with a neural network  $p_\theta(\mathbf{x}_{t-1}|\mathbf{x}_t)$  parameterized by  $\theta$ . It aims to estimate the mean  $\boldsymbol{\mu}_\theta$ , while we fix the covariance to  $\boldsymbol{\Sigma}(\mathbf{x}_t, t) = \frac{1 - \bar{\alpha}_t}{1 - \bar{\alpha}_t} \beta_t \mathbf{I} = \Sigma_t \mathbf{I}$ . The network  $p_\theta(\mathbf{x}_{t-1}|\mathbf{x}_t)$  is trained by maximizing the variational lower bound of the log-likelihood, which can be simplified to several loss terms that mainly consist of KL-divergences between two Gaussians (and are hence computable in closed form) [1].

While the obvious choice is to estimate  $\boldsymbol{\mu}_\theta$ , alternative parameterizations are possible. We can obtain the mean  $\boldsymbol{\mu}_t$  at timestep  $t$  via a combination of the reparameterization trick and Bayes’ theorem [29, 2]:

$$\boldsymbol{\mu}_t(\mathbf{x}_t, \boldsymbol{\epsilon}_t) = \frac{1}{\sqrt{\alpha_t}} \left( \mathbf{x}_t - \frac{\beta_t}{\sqrt{1 - \bar{\alpha}_t}} \boldsymbol{\epsilon}_t \right) = \frac{\sqrt{\alpha_t} (1 - \bar{\alpha}_{t-1})}{1 - \bar{\alpha}_t} \mathbf{x}_t + \frac{\sqrt{\bar{\alpha}_{t-1}} \beta_t}{1 - \bar{\alpha}_t} \mathbf{x}_0, \quad (3)$$

where  $\alpha_t = 1 - \beta_t$ ,  $\bar{\alpha}_t = \prod_{i=1}^t \alpha_i$ , and  $\boldsymbol{\epsilon}_t$  represents Gaussian noise to diffuse  $\mathbf{x}_0$  to  $\mathbf{x}_t$ . Since  $\mathbf{x}_t$  is known during training, predicting  $\boldsymbol{\mu}_t$  fixes the Gaussian noise  $\boldsymbol{\epsilon}_t$  or the clean signal  $\mathbf{x}_0$  and vice versa, and we can equivalently train the model to predict these quantities. While Ho et al. [2] simplified the training to minimize the noise mismatch, we here consider the loss

$$L(\theta) := \mathbb{E}_{t, \mathbf{x}_0, \boldsymbol{\epsilon}} \left[ \lambda_t \|\mathbf{x}_0 - \hat{\mathbf{x}}_0(\mathbf{x}_t(\mathbf{x}_0, \boldsymbol{\epsilon}), t)\|^2 \right], \quad (4)$$

where  $\hat{x}_0$  is the model *estimate* of the clean signal (omitting the parametric dependence on  $\theta$  for conciseness), and  $\lambda_t$  is set to Min-SNR-5 weighting [30].

## 2.2 Assembly of governing equations

Physical laws are typically formulated as a set of PDEs over a domain  $\Omega \subset \mathbb{R}^d$ , expressed as

$$\mathcal{F}[u(\xi)] = 0, \quad \xi = (\xi_1, \xi_2, \dots, \xi_d)^\top \in \Omega, \quad u = (u_1(\xi), u_2(\xi), \dots, u_c(\xi))^\top \in \mathbb{R}^c, \quad (5)$$

with boundary conditions

$$\mathcal{B}[u(\xi)] = 0, \quad \xi \in \partial\Omega, \quad (6)$$

where  $\mathcal{F}$  is a differential operator,  $\mathcal{B}$  is a boundary condition operator,  $\partial\Omega$  is the boundary of domain  $\Omega$ , and  $u$  is the sought solution field that satisfies the set of PDEs for all  $\xi \in \Omega$  and boundary conditions on  $\partial\Omega$ .

We assume that samples generated from the model  $x_0 \sim p_\theta(x_0)$  should satisfy (5) and (6). In this study, we mainly consider image-based architectures common in diffusion models. More formally, we consider a discretized pixel grid  $\Omega^h \subset \mathbb{Z} \times \mathbb{Z}$  (which may serve as an approximation of the continuous domain  $\mathbb{R}^2$ ), where  $\partial\Omega^h$  consists of the boundary pixels. For  $n \times n$  pixels, the model's output is thus defined over  $x_0 \in \mathbb{R}^{c \times n \times n}$ . For instance, in the context of Darcy flow problems in porous media [22],  $x_0$  describes the pressure field or, in the context of solid mechanics, the displacement field [31]. While physics-informed neural networks (PINNs) [26] establish an explicit map  $\mathcal{N} : \xi \mapsto u$  between the input and solution field, which enables the computation of required derivatives for  $\mathcal{F}$  (and potentially  $\mathcal{B}$ ) via automatic differentiation, we here approximate those derivatives via finite differences or comparable methods that directly operate on  $x_0$ . Based on those, we define the average absolute error of a solution field  $x_0$  as

$$\mathcal{R}(x_0) = \frac{1}{M+N} \left( \sum_{i=1}^M |\mathcal{F}_i[x_0]| + \sum_{j=1}^N |\mathcal{B}_j[x_0]| \right), \quad (7)$$

where  $i$  and  $j$  denote the  $i$ -th PDE and  $j$ -th boundary condition constraint, and we consider a total of  $M$  and  $N$  such constraints, respectively.

## 3 Physics-informed diffusion models

We explore a scenario, in which our generative diffusion model must learn a distribution whose samples are to comply with a set of governing equations, i.e.,  $\mathcal{R}(x_0) = 0$ . In the usual data-driven setting, this is only indirectly ensured through the training data, typically collected from a forward simulator that produces data points which inherently follow the governing equations.

The governing equations fully describe the physical system and provide us with, in principle, an *infinite* source of information [32], whereas solved instances  $\{x_0^1, \dots, x_0^n\}$ , posing as training data, represent only a finite set of evaluations in terms of the sought solution fields.<sup>1</sup> While this training data is still valuable since  $\mathcal{R}(x_0) = 0$  is often not easily solved, our strategy is to first state our optimization objective based on the more fundamental governing equations and only subsequently incorporate training data.

### 3.1 Consideration of PDE constraints

We maintain the probabilistic perspective of generative models and introduce the residuals as *virtual observables* [32]  $\hat{r} = 0$ , which we consider to be sampled from the distribution

$$q_{\mathcal{R}}(\hat{r}|x_0) = \mathcal{N}(\hat{r}; \mathcal{R}(x_0), \sigma). \quad (8)$$

In the limit  $\sigma \rightarrow 0$ , this recovers the deterministic setting of strictly enforcing the residual equations, as all probability mass is concentrated in  $\mathcal{R}(x_0)$ . This can be used to compute the virtual likelihood  $p_\theta(\hat{r})$ , which we expand in terms of drawn samples  $x_0$  as

$$p_\theta(\hat{r}) = \int p_\theta(\hat{r}, x_0) dx_0 = \int q(\hat{r}|x_0) p_\theta(x_0) dx_0 = \mathbb{E}_{x_0 \sim p_\theta(x_0)} q(\hat{r}|x_0). \quad (9)$$

<sup>1</sup>Even if we assume access to infinite training samples, the residual information may still be beneficial, since it typically imposes constraints on higher-order derivatives (comparable to Sobolev training [33]).

This factorization of  $p_\theta(\hat{r}, \mathbf{x}_0)$  is reasonable as the residual follows  $\mathbf{x}_0$  via (8). The goal is to maximize the usual log-likelihood over the virtual observable  $\hat{r}$ , i.e.,

$$\arg \max_{\theta} \mathbb{E}_{\hat{r}} [\log p_\theta(\hat{r})] = \arg \max_{\theta} \mathbb{E}_{\mathbf{x}_0 \sim p_\theta(\mathbf{x}_0)} [\log q(\hat{r} = 0 | \mathbf{x}_0)]. \quad (10)$$

Thus, any samples from  $p_\theta(\mathbf{x}_0)$  are evaluated on their log-likelihood via (8), which can also be understood as a probabilistic reinterpretation of the loss used to train PINNs [26].

### 3.2 Consideration of observed data

We emphasize our focus on a *generative* model class in which training data is typically available. This is crucial for two main reasons: first, identifying solutions  $\mathbf{x}_0$  that satisfy the governing equations is non-trivial, and we may understand the obtained training data as guidance for the model towards feasible solutions, which may accelerate the training. Second, (10) contains any distribution that produces samples with zero residuals, and the model may simply collapse to a single solution instance (such as in the classical PINN setup), which is not the use case for a generative scenario. Rather, we aim to leverage the proven capabilities of generative models to learn complex distributions, such as optimal mechanical designs or fluid flows based on some conditioning, while ensuring adherence to the physical laws. Even if no data is available, we may introduce an uninformative prior such as a unit Gaussian to promote the exploration of different solutions, which we briefly investigate in Section 4.1.

We thus extend the objective (10) by including the usual data likelihood term, which is taken as the standard optimization objective in data-driven diffusion models as

$$\arg \max_{\theta} \mathbb{E}_{\mathbf{x}_0 \sim q(\mathbf{x}_0)} [\log p_\theta(\mathbf{x}_0)] + \mathbb{E}_{\mathbf{x}_0 \sim p_\theta(\mathbf{x}_0)} [\log q(\hat{r} = 0 | \mathbf{x}_0)]. \quad (11)$$

It is easy to see that both optimization objectives are *consistent* in the sense that the distribution maximizing the data likelihood also maximizes the virtual (residual) likelihood: the former objective recovers the true distribution  $q(\mathbf{x}_0)$ , which is assumed to model the physical system and generate samples with zero residual, hence also maximizing the latter.

### 3.3 Simplification of the training objective

The joint loss (11) requires sampling not just from  $q(\mathbf{x}_0)$  but also  $p_\theta(\mathbf{x}_0)$ , which in general is costly for diffusion models due to their iterative nature. While much effort has been made to increase inference speed [27, 28], we here aim to simplify (11) to keep changes to the original diffusion model loss minimal. As evident in (3), the model is (directly or indirectly) required to estimate the clean signal  $\hat{\mathbf{x}}_0$  at any given denoising timestep. This estimate aligns with a true sample from  $p_\theta(\mathbf{x}_0)$  only at  $t = 1$  (assuming  $\beta_1 = 0$ ) and becomes progressively less accurate with increasing  $t$ . We leverage this observation and enforce the residual loss on this estimate, which is readily available at any timestep  $t$  via

$$\arg \max_{\theta} \mathbb{E}_{\mathbf{x}_0 \sim q(\mathbf{x}_0)} [\log p_\theta(\mathbf{x}_0)] + \mathbb{E}_{\mathbf{x}_{1:T} \sim p_\theta(\mathbf{x}_{1:T})} [\log q_{\mathcal{R}}(\hat{r} = 0 | \hat{\mathbf{x}}_0(\mathbf{x}_{1:T}))]. \quad (12)$$

To reflect the fact that earlier estimates may be less accurate, we penalize the model less as  $t \rightarrow T$ , and thus model  $q_{\mathcal{R}}(\hat{r} | \hat{\mathbf{x}}_0(\mathbf{x}_{1:T}))$  for simplicity based on a scaled version of the variance scheduler of the reverse process as

$$q_{\mathcal{R}}(\hat{r} | \hat{\mathbf{x}}_0(\mathbf{x}_{1:T})) = \prod_{t=1}^T q_{\mathcal{R}}(\hat{r} | \hat{\mathbf{x}}_0(\mathbf{x}_t, t)), \quad \text{where } q_{\mathcal{R}}(\hat{r} | \hat{\mathbf{x}}_0(\mathbf{x}_t, t)) = \mathcal{N}(\hat{r}; \mathcal{R}(\hat{\mathbf{x}}_0), c\Sigma_t), \quad (13)$$

where  $\Sigma_t$  is, as introduced before, the fixed variance of the denoising process. The scale factor  $c > 0$  effectively dictates the penalty of deviating from  $\mathcal{R}(\hat{\mathbf{x}}_0) = 0$ . Figure 1 shows a graphical illustration of this process.

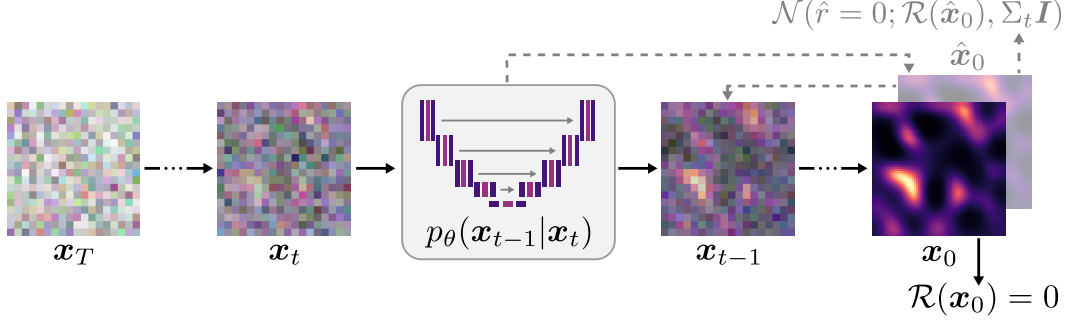


Figure 1: The diffusion model  $p_\theta$  estimates the clean signal  $\hat{x}_0$  throughout the denoising process based on which we evaluate the residual. We tighten the variance of the virtual likelihood as  $t \rightarrow 0$ .

As this still requires sampling over  $\mathbf{x}_{1:T} \sim p_\theta(\mathbf{x}_{1:T})$ , we choose the simplification of directly sampling from  $q(\mathbf{x}_{1:T})$ , effectively ignoring the likelihood ratio, as we aim to minimize

$$\mathbb{E}_{\mathbf{x}_0 \sim q(\mathbf{x}_0)} [-\log p_\theta(\mathbf{x}_0)] + \mathbb{E}_{\mathbf{x}_{1:T} \sim p_\theta(\mathbf{x}_{1:T})} [-\log q_{\mathcal{R}}(\hat{r} = 0 | \hat{\mathbf{x}}_0(\mathbf{x}_{1:T}))] \quad (14)$$

$$\leq \mathbb{E}_{q(\mathbf{x}_{0:T})} \left[ \log \frac{q(\mathbf{x}_{1:T} | \mathbf{x}_0)}{p_\theta(\mathbf{x}_{0:T})} \right] + \mathbb{E}_{\mathbf{x}_{1:T} \sim p_\theta(\mathbf{x}_{1:T})} [-\log q_{\mathcal{R}}(\hat{r} = 0 | \hat{\mathbf{x}}_0(\mathbf{x}_{1:T}))] \quad (15)$$

$$= \mathbb{E}_{q(\mathbf{x}_{0:T})} \left[ \log \frac{q(\mathbf{x}_{1:T} | \mathbf{x}_0)}{p_\theta(\mathbf{x}_{0:T})} \right] + \mathbb{E}_{\mathbf{x}_{1:T} \sim q(\mathbf{x}_{1:T})} \left[ -\frac{p_\theta(\mathbf{x}_{1:T})}{q(\mathbf{x}_{1:T})} \log q_{\mathcal{R}}(\hat{r} = 0 | \hat{\mathbf{x}}_0(\mathbf{x}_{1:T})) \right] \quad (16)$$

$$\approx \mathbb{E}_{q(\mathbf{x}_{0:T})} \left[ \log \frac{q(\mathbf{x}_{1:T} | \mathbf{x}_0)}{p_\theta(\mathbf{x}_{0:T})} \right] + \mathbb{E}_{\mathbf{x}_{1:T} \sim q(\mathbf{x}_{1:T})} [-\log q_{\mathcal{R}}(\hat{r} = 0 | \hat{\mathbf{x}}_0(\mathbf{x}_{1:T}))] \quad (17)$$

$$= \mathbb{E}_{q(\mathbf{x}_{0:T})} \left[ \log \frac{q(\mathbf{x}_{1:T} | \mathbf{x}_0)}{p_\theta(\mathbf{x}_{0:T})} - \log q_{\mathcal{R}}(\hat{r} = 0 | \hat{\mathbf{x}}_0(\mathbf{x}_{1:T})) \right]. \quad (18)$$

We justify this simplification by the assumption that optimizing the variational bound will bring  $p_\theta(\mathbf{x}_{1:T})$  close to  $q(\mathbf{x}_{1:T})$  and thus reduce this bias with ongoing model training. As the original [1] and physics-driven objectives are now under the same expectation, the classical data loss (4) can be straightforwardly extended to include a physics-informed loss, resulting in the loss of our physics-informed diffusion (PIDM) model:

$$L_{\text{PIDM}}(\theta) = \mathbb{E}_{t \sim [1, T], \mathbf{x}_{0:T} \sim q(\mathbf{x}_{0:T})} \left[ \lambda_t \|\mathbf{x}_0 - \hat{\mathbf{x}}_0(\mathbf{x}_t, t)\|^2 + \frac{1}{2\bar{\Sigma}_t^2} \|\mathcal{R}(\hat{\mathbf{x}}_0(\mathbf{x}_t, t))\|^2 \right], \quad (19)$$

where  $\bar{\Sigma}_t = c\Sigma_t$  is the rescaled variance due to  $c$ . Since  $\Sigma_0 = 0$  for a deterministic last step, we set it to  $\Sigma_1$  instead. Algorithm 1 displays the updated training objective, requiring only minor modifications to the standard training setup [2].

---

**Algorithm 1** Physics-informed diffusion model training

---

- 1: Set  $\lambda_t$  for  $t = 1, \dots, T$  and  $\bar{\Sigma}_t = c\Sigma_t$
  - 2: **repeat**
  - 3:    $\mathbf{x}_0 \sim q(\mathbf{x}_0)$
  - 4:    $t \sim \text{Uniform}\{1, \dots, T\}$
  - 5:    $\epsilon \sim \mathcal{N}(\mathbf{0}, \mathbf{I})$
  - 6:    $\mathbf{x}_t = \sqrt{\bar{\alpha}_t} \mathbf{x}_0 + \sqrt{1 - \bar{\alpha}_t} \epsilon$
  - 7:   Take gradient descent step on  $\nabla_\theta \left[ \lambda_t \|\mathbf{x}_0 - \hat{\mathbf{x}}_0(\mathbf{x}_t, t)\|^2 + \frac{1}{2\bar{\Sigma}_t^2} \|\mathcal{R}(\hat{\mathbf{x}}_0(\mathbf{x}_t, t))\|^2 \right]$
  - 8: **until** converged
- 

We point out that the model can still be trained to match the mean or noise as in [2], from which we can equivalently evaluate  $\hat{x}_0$  by (3) to evaluate  $\mathcal{R}(\hat{x}_0)$ . However, we found that this leads to generated samples with larger residual errors compared to directly predicting  $\mathbf{x}_0$ .

### 3.4 Inequality constraints

So far, we have considered PDEs, a special class of equality constraints. Inequality constraints, however, are also common in physics (e.g. thermodynamics laws). Consideration of these constraints of type

$$h(\mathbf{x}_0) \leq h_{\max} \quad (20)$$

can be introduced via  $\mathcal{R}_{\text{ineq}} = \text{ReLU}(h(\mathbf{x}_0) - h_{\max}) = \max(0, h(\mathbf{x}_0) - h_{\max})$ , which we analogously introduce into the variational loss as the Gaussian  $q_{\mathcal{R}_{\text{ineq}}}(\hat{r}_{\text{ineq}} | \hat{\mathbf{x}}_0(\mathbf{x}_t, t)) = \mathcal{N}(\hat{r}_{\text{ineq}}; \mathcal{R}_{\text{ineq}}(\hat{\mathbf{x}}_0), c\mathbf{\Sigma})$  with  $\hat{r}_{\text{ineq}} = 0$ .

### 3.5 Optimization objectives

We may also introduce optimization objectives of the form

$$\min \mathcal{J}(\mathbf{x}_0). \quad (21)$$

As before, we assume this optimum is an available pseudo-observable  $\hat{j}_{\text{opt}}$ , which, unfortunately, is—unlike  $\hat{r}$  and  $\hat{r}_{\text{ineq}}$ —generally unknown. Modeling the virtual likelihood via a Gaussian distribution, however, requires that knowledge<sup>2</sup>. As a remedy, we may introduce the above mismatch as a pseudo-observable sampled from the exponential distribution [32]:

$$\mathcal{J}(\mathbf{x}_0) - \hat{j}_{\text{opt}} \sim \text{Expon}(\lambda), \quad (22)$$

where

$$\text{Expon}(x; \lambda) = \begin{cases} \lambda e^{-\lambda x} & x \geq 0 \\ 0 & x < 0 \end{cases}. \quad (23)$$

By similar reasoning as before, we introduce

$$q_{\mathcal{J}}(\hat{j}_{\text{opt}} | \hat{\mathbf{x}}_0(\mathbf{x}_{1:T})) = \prod_{t=1}^T q_{\mathcal{J}}(\hat{j}_{\text{opt}} | \hat{\mathbf{x}}_0(\mathbf{x}_t, t)), \quad (24)$$

where  $q_{\mathcal{J}}(\hat{j}_{\text{opt}} | \hat{\mathbf{x}}_0(\mathbf{x}_t, t)) = \lambda e^{-\lambda(\mathcal{J}(\mathbf{x}_0) - \hat{j}_{\text{opt}})},$

and observe that the log-likelihood

$$\log q_{\mathcal{J}}(\hat{j}_{\text{opt}} | \hat{\mathbf{x}}_0(\mathbf{x}_{1:T})) = \sum_{t=1}^T \left[ \log(\lambda) - \lambda \mathcal{J}(\hat{\mathbf{x}}_0(\mathbf{x}_t, t)) + \lambda \hat{j}_{\text{opt}} \right] \quad (25)$$

decouples  $\hat{j}_{\text{opt}}$  from  $\hat{\mathbf{x}}_0$ . Therefore, knowledge of  $\hat{j}_{\text{opt}}$  is not required for training. The loss function is hence further extended to

$$L_{\text{PIDM-opt}}(\theta) = \mathbb{E}_{t, \mathbf{x}_{0:T}} \left[ \lambda_t \|\mathbf{x}_0 - \hat{\mathbf{x}}_0(\mathbf{x}_t, t)\|^2 + \frac{1}{2\bar{\Sigma}_t^2} \|\mathcal{R}(\hat{\mathbf{x}}_0(\mathbf{x}_t, t))\|^2 + \lambda \mathcal{J}(\hat{\mathbf{x}}_0(\mathbf{x}_t, t)) \right]. \quad (26)$$

Note that we could also couple the parameter  $\lambda$  of the exponential distribution to the denoising timestep (similar to  $\bar{\Sigma}_t$ ), but chose to keep it constant for now. As usual in multi-objective optimization, trade-offs between the different loss contributions are expected, depending on the relative weighting [34].

## 4 Experiments

### 4.1 Toy problem

**Setup.** In a simple, instructive example, we demonstrate the implications of the proposed physics-informed loss function (19). The objective is to learn a distribution  $q(\mathbf{x})$  that randomly samples points from the unit circle  $\mathcal{S}_1 = \{\boldsymbol{\xi} \in \mathbb{R}^2 : \|\boldsymbol{\xi}\| = 1\}$ , so that samples should obey a simple algebraic equality constraint. We here set  $c = \sqrt{10}$  and thus increase the variance of the implied virtual likelihood. Details of the model architecture and training setup are presented in Appendix A.1.

<sup>2</sup>This is a consequence of the squared exponent in the Gaussian, which couples  $\mathbf{x}_0$  and the virtual observable.

**Results.** To understand the impact of the physics-informed loss, we train the diffusion model in four different scenarios: (i) via the usual variational bound on the data likelihood (4), (ii) via its extension to the residual-informed loss (19), (iii) by only considering the residual loss (and neglecting the variational bound), and (iv) by again considering the residual-informed loss (19) but with data sampled from an uninformative prior  $x_0 \sim \mathcal{N}(\mathbf{0}, \mathbf{I})$ . We present the average residual error of 100 samples generated over 200 training epochs and plot 100 generated samples after training in Figure 2.

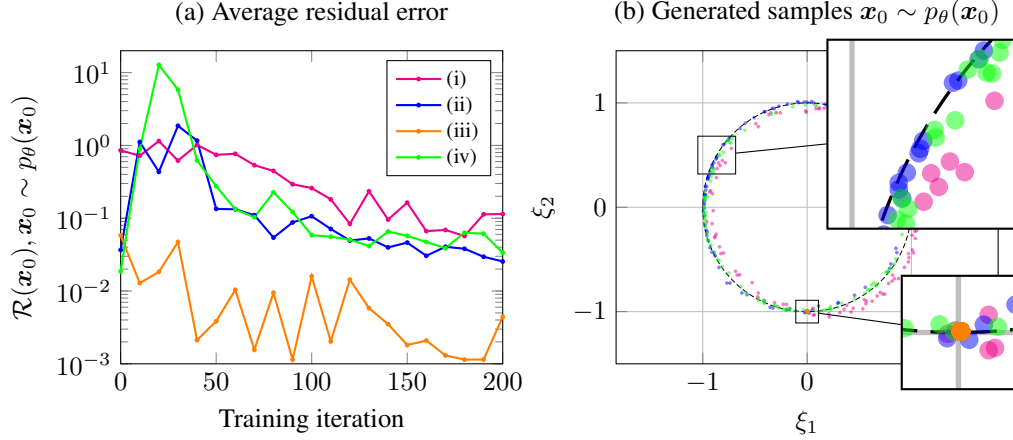


Figure 2: Evaluation of the average residual error of 100 generated samples during training (a) and 100 generated samples after training (b) in four different settings. We consider a diffusion model trained with the standard (data-driven) objective (i), our proposed PIDM (ii), a model trained solely on the residual loss term (iii), and again our proposed PIDM but with data sampled from an uninformative Gaussian prior (iv). In (b), we indicate the unit circle to which all samples should be constrained. Colors in (b) match those in (a).

As indicated in Figure 2a, we observe that the proposed physics-informed loss (ii) indeed outperforms the standard setup (i) in terms of the residual error, particularly noticeable after approximately 40 training epochs. This is also visually confirmed in Figure 2b, where the samples from the “constraint-informed” model align more accurately on the unit circle (see also the top inset). When training the model solely on the constraints (iii), the model efficiently reduces the residual. However, it tends to converge to a single point randomly located somewhere on  $\mathcal{S}_1$ , as shown in the bottom inset. This is indeed expected: the model finds no penalty for collapsing to any points on  $\mathcal{S}_1$ . Interestingly, the model can successfully approximate the target distribution even in the absence of training data using only an uninformative prior (iv). This suggests the use of the uninformative prior as an effective regularization that prompts the model to explore a wider range of solutions within the constraint space. Although the simple setting of this study prevents straightforward analogies to more complex setups, it confirms the validity of our proposed framework and its ability to enforce constraints. We next focus on the more complex scenario of an equality constraint provided by a PDE.

## 4.2 Darcy flow

**Setup.** We study the 2D Darcy flow equations, which describe the steady-state solution for fluid flow through a porous medium, here on a square domain  $\Omega = [0, 1]^2$ . Given a permeability field  $K(\xi)$ , the pressure distribution  $p(\xi)$  and velocity field  $\mathbf{u}(\xi)$  are governed by

$$\begin{aligned} \mathbf{u}(\xi) &= -K(\xi)\nabla p(\xi), \quad \xi \in \Omega \\ \nabla \cdot \mathbf{u}(\xi) &= f(\xi), \quad \xi \in \Omega \\ \mathbf{u}(\xi) \cdot \hat{\mathbf{n}}(\xi) &= 0, \quad \xi \in \partial\Omega \\ \int_{\Omega} p(\xi) d\xi &= 0, \end{aligned} \tag{27}$$

where  $\hat{n}$  denotes the outward unit vector normal to the boundary. Similar to contemporary work [35, 22], we set the source function to

$$f(\boldsymbol{\xi}) = \begin{cases} r, & \text{if } |\xi_i - \frac{1}{2}w| \leq \frac{1}{2}w, \text{ for } i = 1, 2 \\ -r, & \text{if } |\xi_i - 1 + \frac{1}{2}w| \leq \frac{1}{2}w, \text{ for } i = 1, 2 \\ 0, & \text{otherwise,} \end{cases} \quad (28)$$

with  $r = 10$  and  $w = 0.125$ , and we sample  $K(\boldsymbol{\xi})$  from a Gaussian random field (GRF), i.e.,

$$K(\boldsymbol{\xi}) = \exp(G(\boldsymbol{\xi})), \quad G(\cdot) \sim \mathcal{N}(0, k(\cdot, \cdot)) \quad (29)$$

with covariance

$$k(\boldsymbol{\xi}, \boldsymbol{\xi}') = \exp(-\|\boldsymbol{\xi} - \boldsymbol{\xi}'\|_2 / l), \quad \text{with } l = 0.1. \quad (30)$$

Instead of directly considering the GRF, we reduce its dimensionality by considering its Karhunen-Loève expansion up to  $s = 64$  terms,

$$G(\boldsymbol{\xi}) = \sum_{i=1}^s \sqrt{\lambda_i} z_i \phi_i(\boldsymbol{\xi}), \quad (31)$$

with  $\lambda_i$  and  $\phi_i(\boldsymbol{\xi})$  as, respectively, the eigenvalues and eigenfunctions of (30) sorted by decreasing  $\lambda_i$ , and  $z_i \sim \mathcal{N}(0, 1)$ .

We create a training and a validation dataset of 10,000 and 1,000 datapoints, respectively, by solving (27) for a randomly sampled permeability field on a  $64 \times 64$  grid, using second-order central finite differences, giving pairs of  $(\mathbf{K}, \mathbf{p})$  with  $\mathbf{K}, \mathbf{p} \in \mathbb{R}^{n \times n}$ . As shown in detail by Jacobsen et al. [22], this requires solving a system of linear equations. To incorporate the boundary conditions and the integral condition, we extend the linear system of type  $\mathbf{A}\mathbf{p} = \mathbf{f}$  by additionally imposing the above constraints, so that  $\mathbf{A} \in \mathbb{R}^{(n^2+4n+1) \times n^2}$ ,  $\mathbf{p} \in \mathbb{R}^{n^2}$ , and  $\mathbf{f} \in \mathbb{R}^{n^2+4n+1}$  (where  $n = 64$ ). We solve for the over-determined pressure field using SciPy's [36] `linalg.lstsq` solver with default settings.

**Model architecture and residual computation.** We consider a U-Net [37] model architecture based on Phil Wang's implementation [38], given its demonstrated success in learning the denoising process [27]. Our configuration uses an image input resolution of  $64 \times 64$  pixels, aligning with the grid resolution of the linear system under consideration. Importantly, we require the residual evaluation of the predicted images  $\mathcal{R}(\hat{\mathbf{x}}_0)$ , as required in (19), to be consistent with the data, as otherwise the data likelihood would be inconsistent with the (virtual) residual likelihood. This is ensured by using the same finite difference stencils as in the dataset creation, essentially reassembling  $\mathbf{f}$ , except that we remove the integral constraint, since it can be trivially fulfilled by shifting the predicted pressure field [22]. Finite difference stencils are implemented using Pytorch's `nn.Conv2D` [39] layer with a custom kernel, which we can precompute for stencils up to arbitrary order via `findiff` [40].

We here restrict ourselves to an unconditional model, though extensions to conditional generation [41] are straightforward. The U-Net has two in- and output channels and is trained to predict the clean signal based on a noisy input, as stated in Section 2.1. Thus, the model is trained to generate pairs  $(\mathbf{K}, \mathbf{x})$  where  $\mathbf{K}$  is sampled similar to (29), and  $\mathbf{p}$  is the corresponding (unique) pressure field that satisfies the Darcy flow equations (27). We again increase the variance of the virtual residual likelihood by setting  $c = 10$ . Further details of model architecture and training hyperparameters are given in Appendix A.2.

**Results.** To evaluate the performance of our physics-informed diffusion model, we consider three different setups: (i) a model trained on the standard (purely data-driven) objective (4), (ii) a model trained on the standard objective but using residual information as guidance, as described by Shu et al. [12], and (iii) a model similar to (i) but with first-order residual corrections during inference, as described in CoCoGen [22]. Note that the architecture in (ii) differs slightly from the one proposed in [12], but the proposed conditioning mechanism is closely mimicked. For (iii), we first followed the setting proposed in [22] and applied gradient-based descent  $\nabla_{\mathbf{x}_t} \|\mathcal{R}(\mathbf{x}_t)\|_2^2$  with  $\epsilon = 2 \times 10^{-4} / \max \nabla_{\mathbf{x}_t} \mathcal{R}(\mathbf{x}_t)$  for the last  $N$  steps of the sampling iterations and  $M$  additional iterations. We set  $M = 25$  and  $N = 50$  according to the best-reported results (equal to starting corrections halfway through the sampling). However, we encountered stability issues for the above value of  $\epsilon$ , likely due to considering fewer diffusion timesteps than Jacobsen et al [22]. We therefore



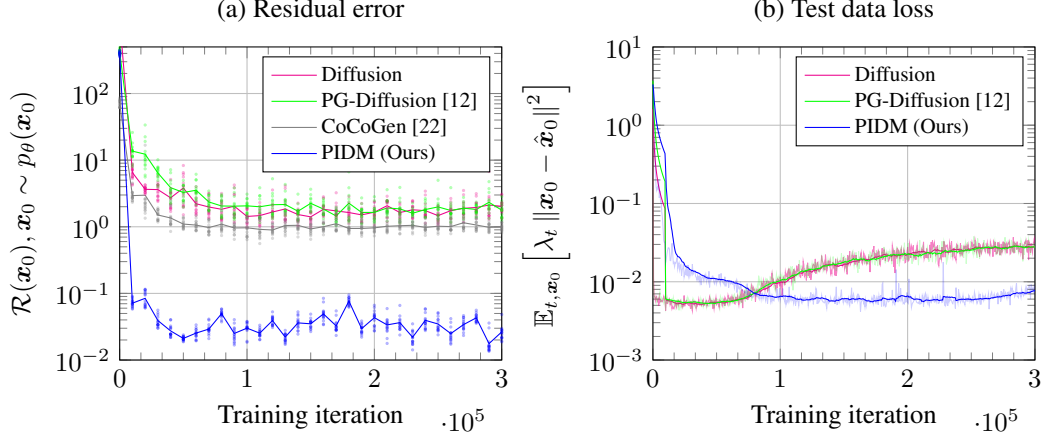


Figure 3: Evaluation of the residual error (a) and test data loss (b) during training. In (a), we generate 16 samples every 10k training iterations and plot the average (solid lines) and individual (dots) residual errors for a standard diffusion model (‘Diffusion’), the physics-guided model (‘PG-Diffusion’) [12], CoCoGen [22], and the proposed physics-informed diffusion model (‘PIDM’). Note that for CoCoGen not all samples converged, so that we excluded the non-converged data from the indicated average. In (b), we plot the data loss evaluated on a test set for those frameworks that differ from ours during training.

conducted a parameter sweep to identify the converging results with the best performance, which we identified<sup>3</sup> at  $\epsilon = 1 \times 10^{-6} / \max \nabla_{x_t} \mathcal{R}(x_t)$ .

We examine the performance of the different diffusion model variants by tracking the evolution of the residual error of generated samples from the learned distributions  $x_0 \sim p_\theta(x_0)$  alongside the test data loss throughout the training process in Figure 3. Our physics-informed diffusion model showcases a remarkable improvement, reducing the residual error by about two orders of magnitude in comparison to the standard diffusion model. By contrast, we could not observe a significant improvement of the residual error for the “physics-guided” model [12]. CoCoGen [22] shows a moderate improvement by reducing the residual by a factor of around 2 but does not bring the residual close to values where the samples could be considered physically consistent. We display some generated samples in Figure 4 for both the standard and physics-informed diffusion models, confirming the drastically reduced residual error over the whole domain.

Figures 3b and 4b-c provide evidence that the physics-informed diffusion model maintains its generative diversity and does not collapse to a single solution instance. It successfully generates permeability (and pressure) fields that adhere to the data distribution (besides respecting the PDE). As our loss function (19) consists of two objectives, a trade-off between the data and residual loss may be expected during training [34], depending on their relative weighting dictated by  $c$ . Interestingly, Figure 3b shows that the test data loss eventually converges to a similar minimum as that of the standard diffusion model, which we attribute to the consistency of these two objectives. Although the physics-informed model requires more iterations to reach the minimum, it is noteworthy that the physics-informed model appears to be significantly less prone to *overfitting* compared to the standard model. We consider this an indicator that the model learns a more robust internal representation of the data distribution, as it is forced to generate samples that adhere to the true distribution or, equivalently, the underlying data generation mechanism—viz. the known constraints that govern the system. Thus, the additional optimization objective may have beneficial effects on the model by enhancing its generalization capability.

<sup>3</sup>While additional sweeps might yield some further incremental improvement, we observed that different values of  $\epsilon$  yielded similar results, as long as the updates converged.

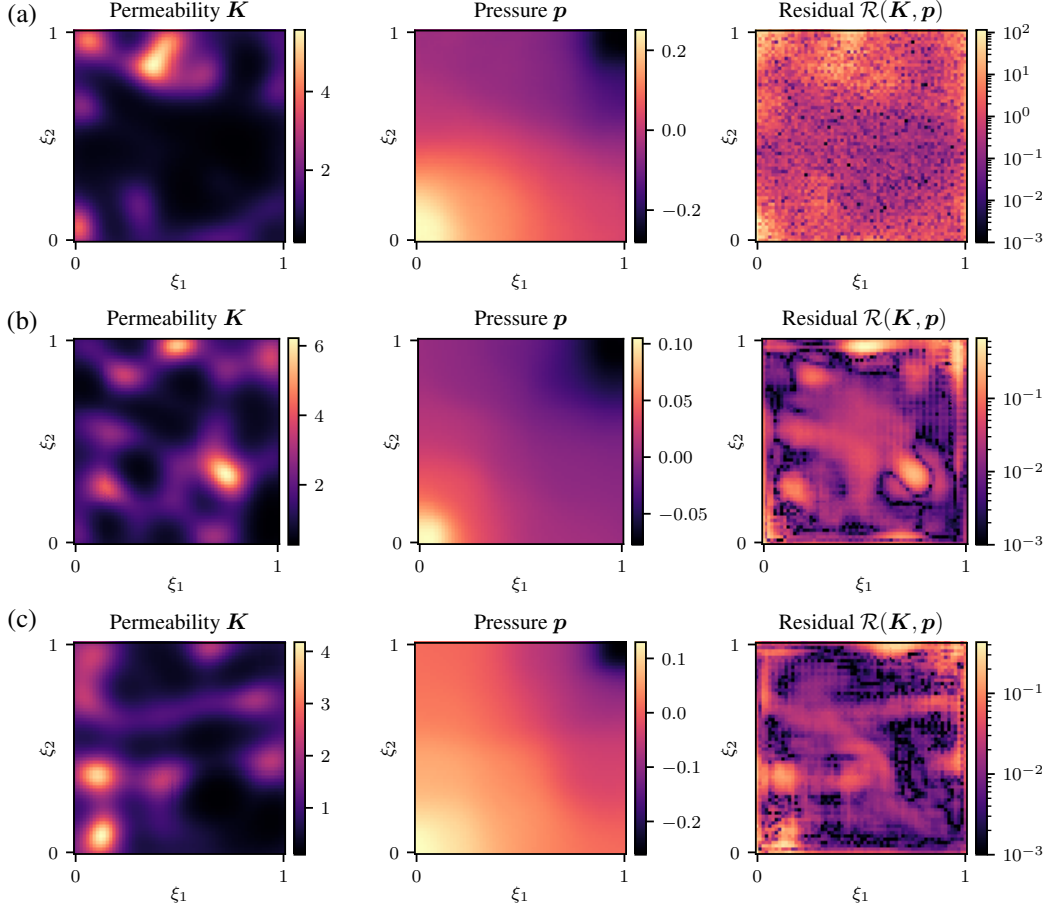


Figure 4: Generated permeability and pressure fields as well as the corresponding residual error from diffusion models trained on the Darcy flow dataset, where (a) is sampled from a standard diffusion model, while samples (b) and (c) are generated via our proposed physics-informed diffusion model.

## 5 Related Work

Conceptually closest to our work are two recent contributions by Shu et al. [12] and Jacobsen et al. [22], as presented in the benchmark in Section 4.2. Shu et al. presented a diffusion model trained to reconstruct high-fidelity flow fields from coarse data and include information on the gradient of the PDE residual to the model in the spirit of classifier-free guidance [41]. We implemented their setup within our framework and could not identify significant improvements over the standard diffusion model. Despite the differences in the PDEs being studied, which limits direct comparisons, we suspect that also their best-reported results (a reduction of the residual of almost one order of magnitude compared to the standard diffusion model) are substantially behind what we report. We hypothesize that the mere inclusion of gradient information into the model seems insufficient because it does not truly enforce residual minimization. Wang et al. [42] optimized the conditioning variable to create an online dataset of soft robot designs, which includes physical performance and may generate samples with improved physical utility. Yet, the focus was on leveraging pre-trained models to create diverse 3D shapes.

Jacobsen et al. [22] presented a strategy to iteratively “correct” the sampled latent variables and the sampled  $x_0$  during the denoising process, utilizing gradient descent on the PDE residuals. As shown in Section 4.2, their approach reduces the residuals of the generated samples, but significantly less than the method proposed here. The key distinction is that we embed physical consistency within the training process rather than as an a-posteriori correction. We highlight that such methods—only

affecting inference—can easily be incorporated into our framework, though we currently see no need to (and the cost of decreased inference speed).

In a broader context, Yuan et al. [24] leveraged diffusion models for human motion synthesis, where inference is altered by projecting the intermediate steps to a physically plausible motion that is verified via a reinforcement learning approach. Similarly, Christopher et al. [23] projected intermediate steps to the closest point in a feasible set, which is generally unknown for more complicated constraints such as PDEs. In general, such post-processing methods may indeed mitigate some of the mismatches of the generated samples (or fulfill them exactly if the constraints are sufficiently simple). Yet, they are fundamentally limited, as they do not address the underlying distribution learned by the model.

## 6 Conclusion

Diffusion models originate from a data-driven perspective and are remarkably successful in approximating high-dimensional data distributions. However, when extending their deployment to scientific machine learning, in which samples generated from such distribution are often required to adhere to specific constraints as imposed by PDEs, diffusion models trained on a purely data-driven objective typically do not reach the required precision. To bridge this gap, we present an extension of the data-driven loss that effectively informs the model on these constraints during training. Our approach significantly reduces the residual error of generated samples compared to the standard setup and earlier frameworks, which predominantly focus on “correcting” the latent variables during inference. Unlike these methods, our strategy ensures that the model internalizes the imposed constraints without compromising the model’s generative abilities. In fact, numerical evidence hints that the physics-informed model obtains a more robust representation of the data distribution that is less prone to overfitting.

The simplicity of our framework allows for straightforward adaptations to other equality or inequality constraints and, additionally, optimization objectives. We hope that this approach stimulates other researchers to extend their generative model training objective when besides data, further information—be it in the form of PDEs or other constraints—on the generated samples is available, as is often the case within the realm of the natural sciences. Future work will be geared toward identifying novel architectures that do not operate on a fixed regular grid, which restricts the work to geometrically simple domains. Inspiration can be found in graph-based architectures that can handle arbitrary meshes [31] or by employing implicit encodings of coordinates [43]. Additionally, coordinate-based representations allow for exact calculation of the gradients required to evaluate the imposed PDEs via automatic differentiation, though at increased computational cost.

## References

- [1] Jascha Sohl-Dickstein, Eric A. Weiss, Niru Maheswaranathan, and Surya Ganguli. Deep Unsupervised Learning using Nonequilibrium Thermodynamics. *ICML*, 2015.
- [2] Jonathan Ho, Ajay Jain, and Pieter Abbeel. Denoising Diffusion Probabilistic Models. *Advances in Neural Information Processing Systems*, (NeurIPS 2020):1–25, 2020.
- [3] Alex Nichol, Prafulla Dhariwal, Aditya Ramesh, Pranav Shyam, Pamela Mishkin, Bob McGrew, Ilya Sutskever, and Mark Chen. GLIDE: Towards Photorealistic Image Generation and Editing with Text-Guided Diffusion Models. 2021.
- [4] Robin Rombach, Andreas Blattmann, Dominik Lorenz, Patrick Esser, and Björn Ommer. High-Resolution Image Synthesis with Latent Diffusion Models. 2021.
- [5] Jonathan Ho, Tim Salimans, Alexey Gritsenko, William Chan, Mohammad Norouzi, and David J. Fleet. Video Diffusion Models. 2022.
- [6] Jonathan Ho, William Chan, Chitwan Saharia, Jay Whang, Ruiqi Gao, Alexey Gritsenko, Diederik P. Kingma, Ben Poole, Mohammad Norouzi, David J. Fleet, and Tim Salimans. Imagen Video: High Definition Video Generation with Diffusion Models. pages 90–91, 2022.
- [7] Chenhao Niu, Yang Song, Jiaming Song, Shengjia Zhao, Aditya Grover, and Stefano Ermon. Permutation Invariant Graph Generation via Score-Based Generative Modeling. 108, 2020.

- [8] Emiel Hoogeboom, Victor Garcia Satorras, Clément Vignac, and Max Welling. Equivariant Diffusion for Molecule Generation in 3D. 2022.
- [9] Xiang Lisa Li, John Thickstun, Ishaan Gulrajani, Percy Liang, and Tatsunori B. Hashimoto. Diffusion-LM Improves Controllable Text Generation. 2022.
- [10] Tong Wu, Zhihao Fan, Xiao Liu, Yeyun Gong, Yelong Shen, Jian Jiao, Hai-Tao Zheng, Juntao Li, Zhongyu Wei, Jian Guo, Nan Duan, and Weizhu Chen. AR-Diffusion: Auto-Regressive Diffusion Model for Text Generation. 2023.
- [11] Zhifeng Kong, Wei Ping, Jiayi Huang, Kexin Zhao, and Bryan Catanzaro. DiffWave: A Versatile Diffusion Model for Audio Synthesis. pages 1–17, 2020.
- [12] Dule Shu, Zijie Li, and Amir Barati Farimani. A physics-informed diffusion model for high-fidelity flow field reconstruction. *Journal of Computational Physics*, 478:111972, 2023.
- [13] Minkai Xu, Lantao Yu, Yang Song, Chence Shi, Stefano Ermon, and Jian Tang. GeoDiff: a Geometric Diffusion Model for Molecular Conformation Generation. (2021):1–19, 2022.
- [14] Tian Xie, Xiang Fu, Octavian-Eugen Ganeva, Regina Barzilay, and Tommi Jaakkola. Crystal Diffusion Variational Autoencoder for Periodic Material Generation. pages 1–20, 2021.
- [15] Christian Dürer, Paul Seibert, Dennis Rücker, Stephanie Handford, Markus Kästner, and Maik Gude. Conditional diffusion-based microstructure reconstruction. *Materials Today Communications*, 35:105608, 2023.
- [16] Jan-Hendrik Bastek and Dennis M. Kochmann. Inverse design of nonlinear mechanical metamaterials via video denoising diffusion models. *Nature Machine Intelligence*, 5(12):1466–1475, 2023.
- [17] Markus J. Buehler. Modeling Atomistic Dynamic Fracture Mechanisms Using a Progressive Transformer Diffusion Model. *Journal of Applied Mechanics*, 89(12), 2022.
- [18] Nikolaos N. Vlassis and WaiChing Sun. Denoising diffusion algorithm for inverse design of microstructures with fine-tuned nonlinear material properties. *Computer Methods in Applied Mechanics and Engineering*, 413:116126, 2023.
- [19] Mohammed Sardar, Alex Skillen, Małgorzata J. Zimoń, Samuel Draycott, and Alistair Revell. Spectrally Decomposed Diffusion Models for Generative Turbulence Recovery. 2023.
- [20] Tianyi Li, Alessandra S. Lanotte, Michele Buzzicotti, Fabio Bonaccorso, and Luca Biferale. Multi-Scale Reconstruction of Turbulent Rotating Flows with Generative Diffusion Models. *Atmosphere*, 15(1):60, 2023.
- [21] Marten Lienen, David Lüdke, Jan Hansen-Palmus, and Stephan Günnemann. From Zero to Turbulence: Generative Modeling for 3D Flow Simulation. 2023.
- [22] Christian Jacobsen, Yilin Zhuang, and Karthik Duraisamy. CoCoGen: Physically-Consistent and Conditioned Score-based Generative Models for Forward and Inverse Problems. pages 1–25, 2023.
- [23] Jacob K Christopher, Stephen Baek, and Ferdinando Fioretto. Projected Generative Diffusion Models for Constraint Satisfaction. 2024.
- [24] Ye Yuan, Jiaming Song, Umar Iqbal, Arash Vahdat, and Jan Kautz. PhysDiff: Physics-Guided Human Motion Diffusion Model. 2022.
- [25] François Mazé and Faez Ahmed. Diffusion Models Beat GANs on Topology Optimization. *Proceedings of the 37th AAAI Conference on Artificial Intelligence, AAAI 2023*, 37:9108–9116, 2023.
- [26] M. Raissi, P. Perdikaris, and G.E. Karniadakis. Physics-informed neural networks: A deep learning framework for solving forward and inverse problems involving nonlinear partial differential equations. *Journal of Computational Physics*, 378:686–707, 2019.

- [27] Prafulla Dhariwal and Alex Nichol. Diffusion Models Beat GANs on Image Synthesis. 2021.
- [28] Ling Yang, Zhilong Zhang, Yang Song, Shenda Hong, Runsheng Xu, Yue Zhao, Wentao Zhang, Bin Cui, and Ming-Hsuan Yang. Diffusion Models: A Comprehensive Survey of Methods and Applications. *ACM Computing Surveys*, 56(4):1–39, 2024.
- [29] Diederik P Kingma and Max Welling. Auto-Encoding Variational Bayes. 2013.
- [30] Tiankai Hang, Shuyang Gu, Chen Li, Jianmin Bao, Dong Chen, Han Hu, Xin Geng, and Baining Guo. Efficient Diffusion Training via Min-SNR Weighting Strategy. 2023.
- [31] Han Gao, Matthew J. Zahr, and Jian Xun Wang. Physics-informed graph neural Galerkin networks: A unified framework for solving PDE-governed forward and inverse problems. *Computer Methods in Applied Mechanics and Engineering*, 390:114502, 2022.
- [32] Maximilian Rixner and Phaedon Stelios Koutsourelakis. A probabilistic generative model for semi-supervised training of coarse-grained surrogates and enforcing physical constraints through virtual observables. *Journal of Computational Physics*, 434, 2021.
- [33] Wojciech Marian Czarnecki, Simon Osindero, Max Jaderberg, Grzegorz Świrszcz, and Razvan Pascanu. Sobolev Training for Neural Networks. 2017.
- [34] Sifan Wang, Yujun Teng, and Paris Perdikaris. Understanding and Mitigating Gradient Flow Pathologies in Physics-Informed Neural Networks. *SIAM Journal on Scientific Computing*, 43(5):A3055–A3081, 2021.
- [35] Yin hao Zhu and Nicholas Zabaras. Bayesian deep convolutional encoder–decoder networks for surrogate modeling and uncertainty quantification. *Journal of Computational Physics*, 366:415–447, 2018.
- [36] Pauli Virtanen, Ralf Gommers, Travis E. Oliphant, Matt Haberland, Tyler Reddy, David Cournapeau, Evgeni Burovski, Pearu Peterson, Warren Weckesser, Jonathan Bright, Stéfan J. van der Walt, Matthew Brett, Joshua Wilson, K. Jarrod Millman, Nikolay Mayorov, Andrew R. J. Nelson, Eric Jones, Robert Kern, Eric Larson, C J Carey, İlhan Polat, Yu Feng, Eric W. Moore, Jake VanderPlas, Denis Laxalde, Josef Perktold, Robert Cimrman, Ian Henriksen, E. A. Quintero, Charles R. Harris, Anne M. Archibald, Antônio H. Ribeiro, Fabian Pedregosa, Paul van Mulbregt, Aditya Vijaykumar, Alessandro Pietro Bardelli, Alex Rothberg, Andreas Hilboll, Andreas Kloeckner, Anthony Scopatz, Antony Lee, Ariel Rokem, C. Nathan Woods, Chad Fulton, Charles Masson, Christian Häggström, Clark Fitzgerald, David A. Nicholson, David R. Hagen, Dmitrii V. Pasechnik, Emanuele Olivetti, Eric Martin, Eric Wieser, Fabrice Silva, Felix Lenders, Florian Wilhelm, G. Young, Gavin A. Price, Gert-Ludwig Ingold, Gregory E. Allen, Gregory R. Lee, Hervé Audren, Irvin Probst, Jörg P. Dietrich, Jacob Silterra, James T Webber, Janko Slavič, Joel Nothman, Johannes Buchner, Johannes Kulick, Johannes L. Schönberger, José Vinícius de Miranda Cardoso, Joscha Reimer, Joseph Harrington, Juan Luis Cano Rodríguez, Juan Nunez-Iglesias, Justin Kuczynski, Kevin Tritz, Martin Thoma, Matthew Newville, Matthias Kümmerer, Maximilian Bolingbroke, Michael Tartre, Mikhail Pak, Nathaniel J. Smith, Nikolai Nowaczyk, Nikolay Shebanov, Oleksandr Pavlyk, Per A. Brodtkorb, Perry Lee, Robert T. McGibbon, Roman Feldbauer, Sam Lewis, Sam Tygier, Scott Sievert, Sebastiano Vigna, Stefan Peterson, Surhud More, Tadeusz Pudlik, Takuya Oshima, Thomas J. Pingel, Thomas P. Robitaille, Thomas Spura, Thouis R. Jones, Tim Cera, Tim Leslie, Tiziano Zito, Tom Krauss, Utkarsh Upadhyay, Yaroslav O. Halchenko, and Yoshiki Vázquez-Baeza. SciPy 1.0: fundamental algorithms for scientific computing in Python. *Nature Methods*, 17(3):261–272, 2020.
- [37] Olaf Ronneberger, Philipp Fischer, and Thomas Brox. U-Net: Convolutional Networks for Biomedical Image Segmentation. 2015.
- [38] Phil Wang. Implementation of Imagen, Google’s Text-to-Image Neural Network that beats DALL-E2, in Pytorch, 2022.
- [39] Adam Paszke, Sam Gross, Francisco Massa, Adam Lerer, James Bradbury, Gregory Chanan, Trevor Killeen, Zeming Lin, Natalia Gimelshein, Luca Antiga, Alban Desmaison, Andreas Köpf, Edward Yang, Zach DeVito, Martin Raison, Alykhan Tejani, Sasank Chilamkurthy,

- Benoit Steiner, Lu Fang, Junjie Bai, and Soumith Chintala. PyTorch: An imperative style, high-performance deep learning library. *Advances in Neural Information Processing Systems*, 2019.
- [40] Matthias Baer. findiff Software Package, 2018.
  - [41] Jonathan Ho and Tim Salimans. Classifier-Free Diffusion Guidance. 2022.
  - [42] Tsun-hsuan Wang, Juntian Zheng, Pingchuan Ma, Yilun Du, Byungchul Kim, Andrew Spielberg, Joshua Tenenbaum, Chuang Gan, and Daniela Rus. DiffuseBot: Breeding Soft Robots With Physics-Augmented Generative Diffusion Models. (1830901):1–26, 2023.
  - [43] Hongying Liu, Zekun Li, Fanhua Shang, Yuanyuan Liu, Liang Wan, Wei Feng, and Radu Timofte. Arbitrary-scale super-resolution via deep learning: A comprehensive survey. *Information Fusion*, page 102015, 2023.
  - [44] Diederik P. Kingma and Jimmy Ba. Adam: A Method for Stochastic Optimization. *3rd International Conference on Learning Representations, ICLR 2015 - Conference Track Proceedings*, pages 1–15, 2014.
  - [45] Yuxin Wu and Kaiming He. Group Normalization. 2018.
  - [46] Stefan Elfving, Eiji Uchibe, and Kenji Doya. Sigmoid-Weighted Linear Units for Neural Network Function Approximation in Reinforcement Learning. 2017.
  - [47] Jimmy Lei Ba, Jamie Ryan Kiros, and Geoffrey E. Hinton. Layer Normalization. 2016.
  - [48] Ashish Vaswani, Noam Shazeer, Niki Parmar, Jakob Uszkoreit, Llion Jones, Aidan N. Gomez, Lukasz Kaiser, and Illia Polosukhin. Attention Is All You Need. 2017.
  - [49] Angelos Katharopoulos, Apoorv Vyas, Nikolaos Pappas, and François Fleuret. Transformers are RNNs: Fast Autoregressive Transformers with Linear Attention. 2020.

## A Model architecture and training

### A.1 Toy problem

We choose a simple 3-layer MLP of latent dimension 128 with a 2D vector  $(\xi_1, \xi_2)$  as in- and output. Information about the diffusion timestep  $t$  is added by transforming  $t$  to an embedding which is element-wise multiplied by the output of the linear layer, generally followed by the Softplus activation (except for the last layer). We train the model for 200 epochs on 10,000 randomly sampled points of the unit circle, using the Adam optimizer [44] with a learning rate of 0.001. We use a batch size of 128, and 100 diffusion timesteps with a cosine scheduler [27].

### A.2 Darcy flow

As described in Section 4.2 we consider a U-Net-based architecture [37]. The main model and training hyperparameters are summarized in Tables 1 and 2, respectively. The model is implemented and trained using PyTorch [39]. Further details can be found in the code repository, which is released upon publication.

Table 1: Denoising diffusion architecture hyperparameters.

Hyperparameter	Value
In- and output channels (Darcy flow)	2, 2
ResNet blocks per down- and upsampling pass	2
ResNet block normalization	Group Normalization [45]
ResNet block activation function	SiLU [46]
Attention block normalization	Layer Normalization [47]
Feature map resolutions (downsampling pass)	$64 \times 64 \rightarrow 32 \times 32 \rightarrow 16 \times 16 \rightarrow 6 \times 6$
Latent dimensions (in feature maps)	$32 \rightarrow 64 \rightarrow 128 \rightarrow 256$
Attention [48, 49] head dimension	32
Number of attention heads	8

Table 2: Diffusion process and training hyperparameters.

Hyperparameter	Value
Diffusion timesteps	100
$\beta_t$ -scheduler	Cosine schedule [27]
Training data size	10,000
Validation data size	1,000
Batch size	64
Learning rate	$10^{-4}$
Optimization algorithm	Adam [44]
EMA start (iteration)	1,000
Exponential Moving Average (EMA) decay	0.99
Dropout	none